Journal of Materials Chemistry A

Accepted Manuscript

ROYAL SOCIETY OF CHEMISTRY

www.rsc.org/materialsA

Laser induced nucleation of plasmonic nanoparticles on two-dimensional nanosheets for organic photovoltaics

M. Sygletou[1,2], P. Tzourmpakis[3,4], C. Petridis[3,5] , D. Konios[3,6], C. Fotakis[1,2], E. Kymakis[3*] and E. Stratakis[1,4*]

[1] Institute of Electronic Structure and Laser, Foundation for Research and Technology - Hellas, Heraklion, 71110, Crete, Greece Email: stratak@iesl.forth.gr

[2] Department of Physics, University of Crete, Heraklion, 71003, Crete, Greece

[3] Center of Materials Technology and Photonics & Electrical Engineering Department, Technological Educational Institute (TEI) of Crete, Heraklion, 71004 Crete, Greece Email: kymakis@staff.teicrete.gr

[4] Department of Materials Science and Technology, University of Crete, Heraklion, 71003 Crete, Greece

[5] Department of Electronic Engineering, Technological Educational Institute (TEI) of Crete, Chania, 73135, Crete, Greece

[6] Department of Chemistry, University of Crete, Heraklion, 71003 Crete, Greece

Abstract

A novel top-down and universal optical technique for the effective decoration of two-dimensional (2D) nanosheets (NS), of graphene oxide (GO), boron nitride (BN) and tungsten disulfide (WS_2), with noble metallic nanoparticles (NPs) is reported. The NS-NPs assemblies were formed under ambient conditions, via a facile, rapid and solution compatible laser assisted process in the presence of a metallic precursor. It is shown that a few seconds of irradiation is sufficient to decorate the NS lattice, while the NPs density can be readily controlled upon variation of the irradiation time. It is found that the laser induced anchoring of Au NPs onto NS basal plane and edges resulted in enhanced light harvesting that is potentially useful for energy conversion and storage applications. To demonstrate the potential of the approach for practical applications, the incorporation of WS_2-Au NPs assemblies into the photoactive layer of ternary bulk heterojunction (BHJ) organic photovoltaic (OPV) cells is realized. The power conversion efficiency (PCE) of the binary device consisting of a poly[N-9'-heptadecanyl-2,7-carbazole-alt-5,5-(4',7'-di-2-thienyl-2',1',3'-benzothiadiazole)] (PCDTBT):[6,6]-phenyl-C71-butyric-acid-

methyl-ester ($PC_{71}BM$) blend as the donor-acceptor pair was 5.6%, while after the employment of WS_2-Au NPs the efficiency enhancement of the ternary device was approximately 13% reaching a total PCE of 6.3%. The facile, rapid and room temperature nature of the photo-induced method proposed here provides unique opportunities for the cost-effective synthesis of bulk amounts of NS-NPs assemblies in solution for many optoelectronic applications.

Introduction

The interest on 2D materials has been rapidly raised since 2004 when Novoselov and Geim isolated one atomic layer thick graphene sheets, revealing their extraordinary properties and great potential for various applications[1]. Transition metal dichalcogenides (TMDCs) with the common structural form MeX_2 (Me = Mo, W, Ti, etc and X = S, Se, Te), and boron nitride (BN) NS exhibit a laminar structure similar to that of graphene and have drawn the attention of research community[2,3,4,5]. One of the most attractive features of TMDCs structured compounds is their transition from indirect band gap semiconductors in their bulk nature, to direct band gap semiconductors when isolated as a monolayer. In particular, their electrical properties vary from metals to wide band gap semiconductors depending on the number of layers involved in the sheet, while they can be easily tuned by modification of the crystal structure or by applying strain.[6] The tungsten disulfide (WS_2) and molybdenum disulfide (MoS_2) are semiconductors with band gaps ranging from the visible to the near-infrared[7]. While, hexagonal BN is an excellent dielectric.[4]

On the other hand, noble metal nanoparticles (NPs) such as Au, Ag and Pt are of great interest because of their unique physical and chemical properties. Such properties are strongly dependent on their size and shape and therefore much attention has been paid to exploit such effects for potential applications. Accordingly, numerous applications have been demonstrated, ranging from plasmonic optoelectronic devices[8,9,10] to catalysis[11,12,13] and nonlinear photonic devices[14,15,16,17]. Another challenging application is in the field of organic photovoltaics (OPVs), where plasmonic NPs have been extensively used for solar light harvesting and, in turn, for OPV efficiency enhancement.[18] Specifically, when the NPs diameter is smaller than 40 nm, NPs act as sub-wavelength antennas, leading to enhanced light absorption due to plasmon resonance

effect.[19,20] Larger diameter NPs function as multiple scattering centers, giving rise to increase of the optical path length within the photoactive medium.[21,22,23].

In this context, the possibility of incorporating solution processable 2D materials combined with metal NPs to form NS-NPs assemblies inside the photoactive layer of OPVs can provide a dual enhancement effect. Firstly, the NPs will enhance the light absorption via either plasmonic or scattering effects, and secondly the bandgap tunability 2D NS could give rise to enhanced exciton dissociation and charge collection through the formation of a ternary OPV configuration[24]. Apart from the benefits in OPV technology, the development of NS-NPs assemblies in solution could further allow the realization of various printable nanophotonic devices with tunable optical and electronic properties, covering a wide spectral range from the microwave to the ultraviolet. For example, the decoration of MoS_2 NS with Au NPs has led to a p-doping effect in MoS_2 NS transistors[25] as well as to plasmon enhanced photocatalytic water splitting[26].

In this paper we introduce a one-step, in situ laser induced anchoring of noble metallic NPs onto the surface area of thin 2D NS and demonstrate the potential use of such assemblies in OPV applications. The method involves the UV laser irradiation of NS dispersions in the presence of a precursor metallic salt. The preparation is based on photo-activation of NS surface by UV laser photons, followed by chemical reduction of the metallic precursor.[27] Although several methods have been reported for the laser-assisted synthesis of graphene- and GO-NPs nanocomposites, currently there is no report, to our knowledge, on the laser-induced formation of metallic NPs onto other kinds of 2D NS.[28,29,30,31] Therefore, our approach is universal, i.e the NPs anchoring can be realised in different types of NSs including GO, WS_2, MoS_2 and BN. It is important that this one-step, room temperature, synthesis is achieved in the absence of surfactants, catalysts or toxic chemical reducing agents thus providing a green approach for the synthesis of NS-NPs nanocomposites. Furthermore, it is faster and more efficient compared to the previously reported techniques, considering that a single laser pulse is sufficient to obtain stable 2D-NPs dispersions. Finally, as a proof of concept, the novel application of hybrid 2D-NPs materials in ternary organic photovoltaic (OPV) is demonstrated. It is found that the WS_2 NS decorated with plasmonic Au NPs could function as an efficient additive into ternary OPV devices. It is shown that the incorporation of WS_2 NS-Au NPs assemblies into the PCDTBT:$PC_{71}BM$ active layer of OPV cells gives rise to a conversion efficiency enhancement of ~13% with respect to reference

devices, a result that demonstrates the potential use of laser-decorated plasmonic 2D materials for further optoelectronic applications.

2. Experimental Details

2.1 Reagents and materials

The pristine NS were purchased from Graphene Supermarket in dispersions (GO=500 mg L^{-1}, BN=5.4 mg L^{-1}, WS_2=26 mg L^{-1}). The BN flake lateral size was 50-200 nm consisting of 1 to 5 monolayers. The WS_2 flake lateral size was 50-150 nm and they were consisted of 1 to 4 monolayers. The size of GO flakes was 0.3-0.7 μm consisting of at least 80% monolayers. The chloroauric acid ($HAuCl_4$, ethanol as solvent) and silver nitrate ($AgNO_3$, distilled water as solvent) salts were supplied from Sigma Aldrich.

2.2 Laser irradiation process

Mixed dispersions of NS with $HAuCl_4$ in ethanol or $AgNO_3$ in water were placed into a quartz cuvette and were subjected to illumination by excimer laser UV pulses (wavelength of 248 nm, 20 ns pulse duration). A couple of irises secured the formation of a spatially uniform laser beam spot of 8.5 mm diameter that illuminated the solution. Two different irradiation fluences were used, 100 mJ/cm^2 or 1000 mJ/cm^2, corresponding to a single pulse power of 56.7 mW and 567 mW respectively. During illumination, the irradiated dispersions were continuously agitated via a magnetic stirrer. A schematic representation of the experimental process is depicted in **Figure 1A**. To investigate the process of the laser induced NPs anchoring onto NS, the irradiation power, the number of pulses and the relative concentration of NS over the salt precursor were varied.

2.3 Materials characterization

Characterization was carried out after purification by three centrifugation/decantation and re-dispersion steps to ensure that any non-covalently attached NPs were removed. In particular, the morphology of pristine and NPs' decorated NS was characterized with High Resolution Transmission Electron Microscopy (HRTEM), using a JEOL-2100 LaB_6 ultra-high-resolution electron microscope. The UV-Vis absorption spectra of the initial and laser-irradiated solutions were obtained using a Perkin Elmer, LAMBDA 950 UV/VIS/NIR spectrophotometer. Raman spectroscopy is performed at room temperature using a Nicolet Almega XR Raman spectrometer

equipped with a 470 nm laser as an excitation source. For the preparation of the samples, the NS and NS-NPs assemblies were drop casted onto quartz substrates.

2.4 Devices fabrication and characterization

PCDTBT and $PC_{71}BM$, both purchased from Solaris Chem, were dissolved in 1,2-dichlorobenzene:chlorobenzene (3:1) (o-DCB:CB), with a 1:4 (4 mg:16 mg) ratio and stirred overnight at 70 °C. The resulting PCDTBT:$PC_{71}BM$ solutions were mixed with different amounts of WS_2 and WS_2-Au NS (1.0%, 1.5%, and 2.5% v/v) to obtain the final blends. The photovoltaic devices were fabricated onto 20 mm by 15 mm indium-tin-oxide (ITO) on glass substrates with a sheet resistance of ~20 Ω sq^{-1}. The impurities are removed from the ITO glass through a 3-step cleaning process (soap solution, acetone and isopropanol). WS_2 and WS_2-Au NS were also dissolved into o-DCB followed by utrasonication for 1 h. Following this cleaning process, the substrates were spin-casted with a poly (3,4-ethylenedioxythiophene):poly (styrene sulfonate) (PEDOT:PSS) layer at 6000 rpm for 60 s, obtaining a 30 nm hole transport layer. The films were baked for 20 min at 120 °C inside a nitrogen-filled glove box to dry any residual moisture. All photoactive layers (PCDTBT:$PC_{71}BM$ and PCDTBT:$PC_{71}BM$:WS_2 and PCDTBT:$PC_{71}BM$:WS_2:Au) were subsequently deposited on top of the PEDOT:PSS layer by spin-coating at 1000 rpm, until the thickness reached approximately 80 nm determined by cross-sectional SEM images. The cells were dried at 60 °C for 1 min and subsequently a 10 nm Ca interlayer and a 100 nm Al top electrode were deposited through a shadow mask by thermal evaporation to complete device architecture, creating an active area of 0.04 cm^2.

The optoelectronic performance of the solar cell devices were measured at room temperature with an Air Mass 1.5 Global (A.M. 1.5 G) solar simulator at an intensity of 100 mW cm^{-2} inside a glove box. Current–voltage (J–V) measurements were performed using an Agilent B1500A Semiconductor Device Analyzer. A reference monocrystaline silicon solar cell from Newport was used to calibrate the light intensity. The external quantum efficiency (EQE) measurements were conducted immediately after device fabrication and encapsulation method because of the sensitivity of Ca on air conditions. The respective EQE spectra were monitored using a Xe lamp passing through a monochromator and an optical chopper at low frequencies (~200 Hz) in order to maximize the signal/noise (S/N) ratio.

3. Results and discussion

3.1 Synthesis of 2D NSs-NPs assemblies

The laser-induced reaction leading to NPs nucleation onto the 2D NS took place into a quartz cuvette, containing the initial NS dispersion into which the precursor molecules were dissolved. The efficiency of the process was unexpectedly high, as the final product was delivered via irradiation with a single laser pulse. In order to find out the optimum parameters for the NS decoration a series of different volume ratios of NS over precursor solution were investigated.

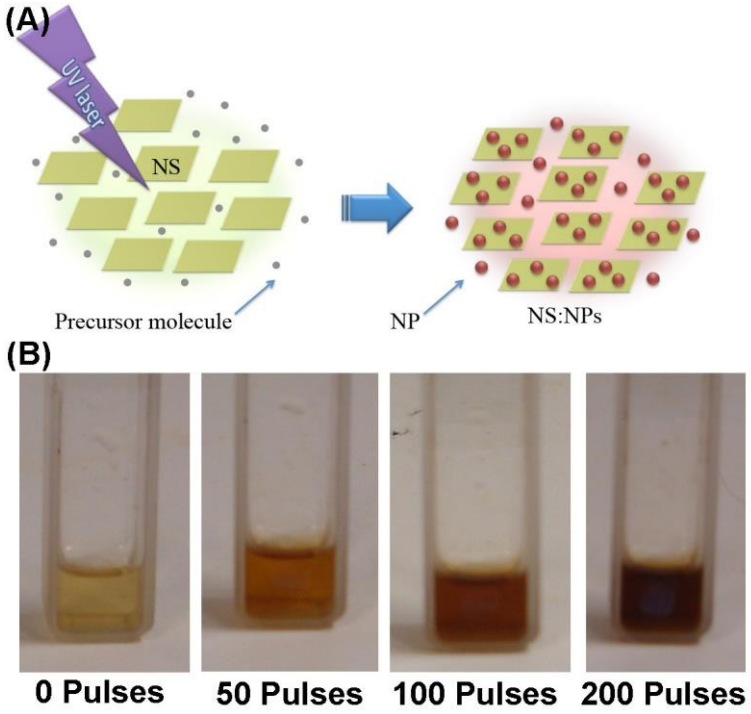

Figure 1: A) Schematic of the experimental process of laser-induced generation of NS:NPs assemblies; B) Pictures of the reference and laser treated GO-$HAuCl_4$ dispersions, irradiated with different numbers of 100mJcm^{-2} UV pulses.

The best results, as far as the uniformity of NS decoration and the stability of the final solutions against precipitation, were obtained for NS:precursor ratios of 1:1, 1:2 and 1:4 respectively, using two different laser fluences of 100 or 1000 mJcm^{-2}. It should be emphasized that the irradiated dispersions were stable, since no precipitation is observed even after months of storage in ambient conditions.

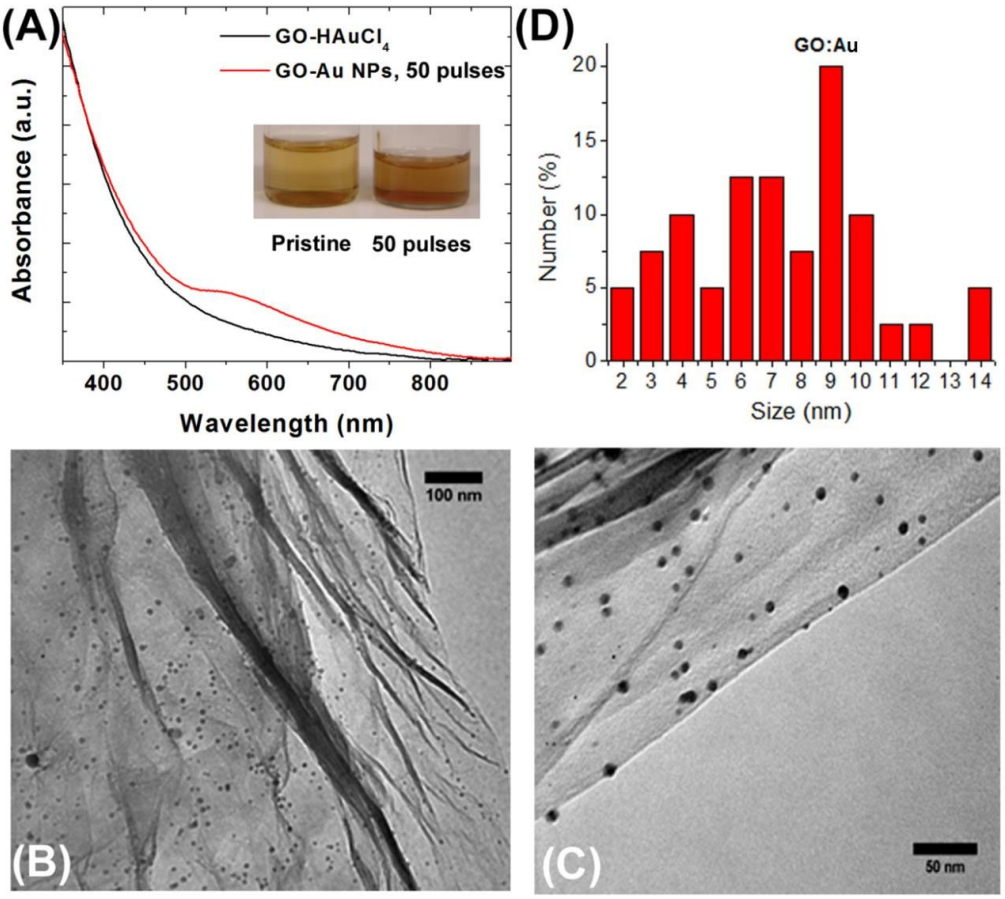

Figure 2: (A) UV-vis absorption spectra of pristine GO-$HAuCl_4$ dispersions in ethanol before (black line) and after irradiation with 50 UV laser pulses of 100mJcm^{-2}. The inset depicts an image of the respective dispersions; (B), (C): TEM images of the GO-Au assemblies after the illumination of the mixed solutions at ratio 2:1 with a single UV pulse and fluence of 100 mJ cm^{-2}; (D) Size distribution of the Au NPs grafted onto the GO NSs.

In a first experiment we have irradiated GO NS in the presence of $HAuCl_4$ metallic precursor. As the GO NS surface was activated and decorated with Au NPs, upon irradiation with consecutive UV pulses, the coloration of the mixture was gradually turned from bright yellow to dark red (**Figure 1B)**. The corresponding UV-vis spectra of GO-Au assemblies formed are presented in **Figure 2A**. As expected, the spectrum shows the appearance of a distinct peak at 545 nm, corresponding to the surface plasmon resonance (SPR)[32] of gold NPs. We postulate that the photo-reduction of the $HAuCl_4$ solution was the main source of NPs generation. Similar results were obtained in the case of GO-Ag assemblies formed upon irradiation of GO-NS-

$AgNO_3$ dispersions (**Fig. S1**, electronic supplementary information (ESI)). In this case as well, following an elevated number of pulses, a characteristic peak at ~400 nm appeared in the UV-vis spectrum of the irradiated dispersion, corresponding to the SPR of Ag NPs.[33]

Further evidence that the NPs were successfully grafted onto GO NS was obtained by TEM imaging. **Figures 2B, C** shows typical TEM images of GO:Au assemblies formed using a single UV laser pulse of 100 mJ cm^{-2}. It is clear that NPs are uniformly distributed on the NS surface. The corresponding size distribution of the nucleated Au NPs is presented in **Figure 2D**. **Figures S2** and **S3** show the respective TEM images and size distribution for Ag NPs.

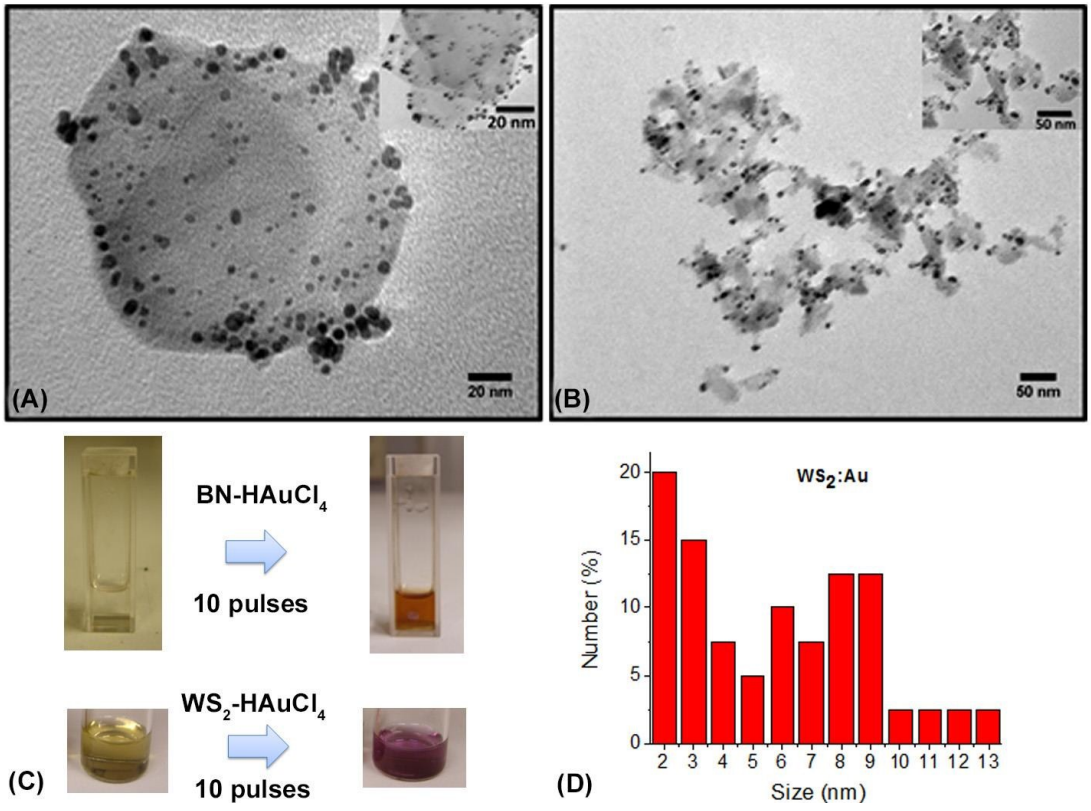

Figure 3: TEM images of BN-Au (A) and WS_2-Au (B) NPs assemblies following the illumination of the mixed solutions (ratios 1:4 and 1:2 respectively), with a single UV pulse and fluence of 100 mJ cm^{-2}; (C) Pictures of the pristine and laser irradiated dispersions; (D) Size distribution of the Au NPs grafted onto the WS_2 NS, produced by a single, of 100mJcm^{-2}, UV pulse.

The laser-assisted assembly of NPs can be universally applied to other 2D NS such as WS_2, MoS_2 and BN. **Figures 3A, B** and **S7** shows the respective TEM images for BN-Au and WS_2-Au and MoS_2-Au assemblies respectively, synthesized via irradiation of 1:1 mixture solutions with a single pulse of 100 mJ cm^{-2} fluence. As in the case of GO gold NPs were uniformly dispersed onto the NSs surface. The corresponding NPs size distributions can be shown in **Figure 3D** for WS_2:Au and **Figures S8, 10** for MoS_2-Au and BN-Au respectively; in all cases the NPs size ranged from ~1 to ~15 nm.

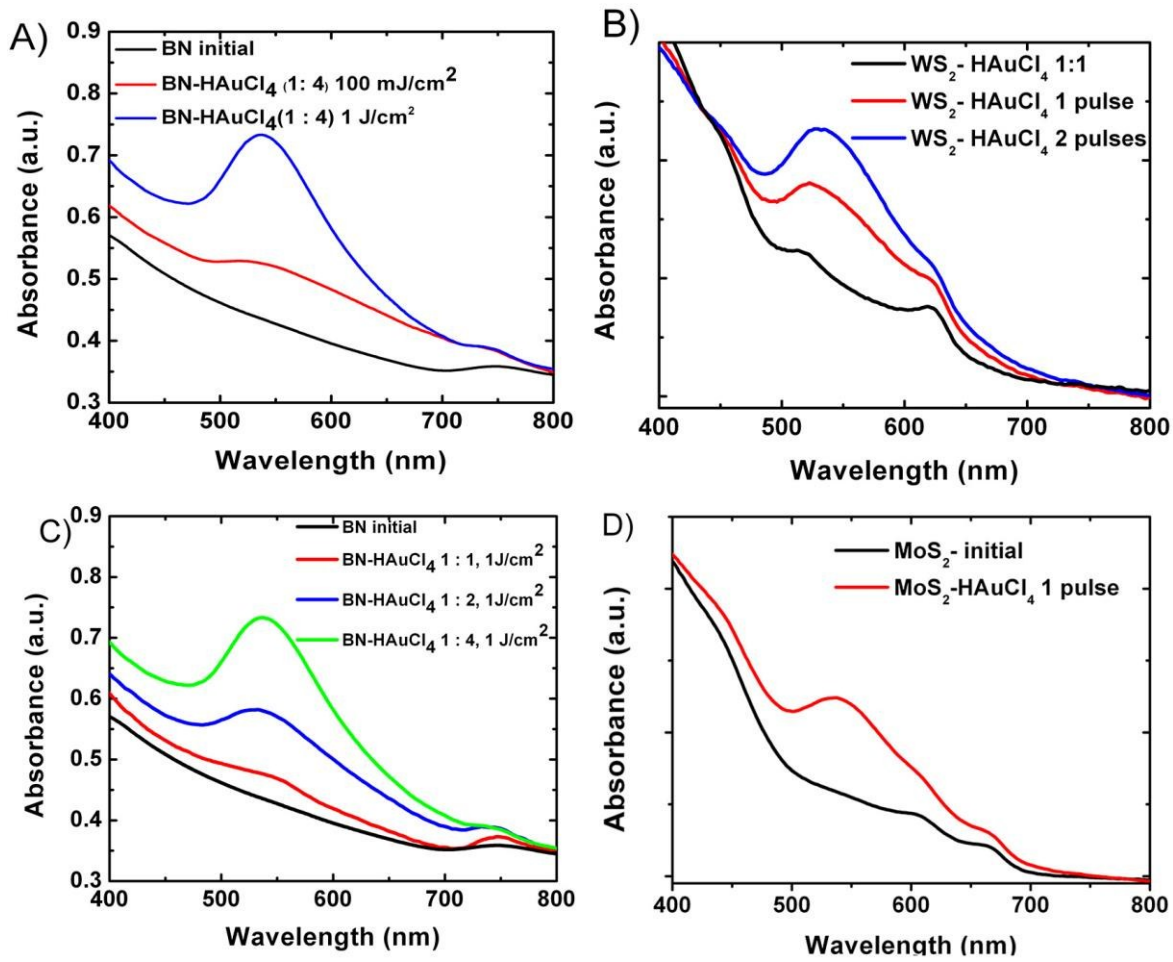

Figure 4. UV-Visible absorption measurements of laser illuminated a) BN-$HAuCl_4$ and b) WS_2-$HAuCl_4$ solutions with different laser fluences. UV-Visible absorption measurements of laser illuminated c) BN-$HAuCl_4$ and d) WS_2-$HAuCl_4$ solutions, with different relative concentrations.

To further investigate the process of the laser induced NPs anchoring onto NS, the irradiation power, the number of pulses and the relative concentration of NS over the salt precursor were

varied. **Figure 4** depicts representative UV-Vis absorption spectra of laser treated BN-$HAuCl_4$ (**Figs. 4A and C**), and WS_2-$HAuCl_4$ (**Fig. 4B**) MoS_2-$HAuCl_4$ (**Fig. 4D**) dispersions at different laser fluences, number of pulses and different NS:precursor relative concentrations. A general trend is that as one increases the fluence or the pulse number or the NS:precursor ratio, the gold plasmon resonance peak becomes more pronounced. TEM imaging (not shown) revealed that the density of NPs anchored onto NSs increases accordingly. Similar results were obtained in the case of NS-Ag NPs assemblies (**Figs S5, S6, S9)**.

Raman spectroscopy was employed in order to identify any laser induced structural modification of the laser treated NS dispersions. The Raman spectra of GO-Ag and GO-Au NSs, presented in **Figure S11A**, indicate that the molecular structure of GO NSs had not been affected by the laser induced synthetic process. As a result, the characteristic G and D Raman peaks of GO at 1313 cm^{-1} and 1585 cm^{-1} showed no significant changes following the irradiation process. A similar observation was made in the case of the laser synthesized WS_2-Au NSs. Indeed, the Raman spectra of the NSs before and after single pulse UV laser irradiation do not indicate any significant differences. **Figure S11B** presents the respective spectra showing the characteristic E_{2g} and A_{1g} modes of WS_2 at 355 cm^{-1} and 418 cm^{-1} respectively. Finally, the pristine and Au NPs decorated BN NSs demonstrate a basic Raman peak at 1363 cm^{-1}, which is the characteristic peak of the hexagonal BN (h-BN) phase (**Figure S11C**)[34]. The second peak appeared at around 1050 cm^{-1} corresponds to the translational optical (TO) vibrational mode of the crystalline BN (c-BN) phase. Both peaks showed no significant difference upon laser irradiation. The above results indicate that the assembly of NPs onto NSs surface occurs without inducing any chemical modification to the pristine 2D NS.

Based on the above observations we may propose a mechanism behind the laser-induced formation of NSs surface. Oxygen groups, which are always present in exfoliated 2D NSs in water, contribute to an overall negatively charged NS surface[30,35,36]. This negative charging effect is responsible for the attachment of the free Au^{3+} ions in $HAuCl_4^-$ or Ag+ ions in $AgNO_3$ aqueous solutions due to electrostatic interactions. Subsequently, the UV laser pulse supplied the energy to facilitate the reduction of such ions, via charge transfer from the NSs to the ions, enabling the growth of NPs onto the NSs surface[37,38]. Based on the above, it is reasonable to suggest that oxygen functional groups are acting as nucleation sites for the UV-assisted growth of the metal

NPs onto the NS surface. Alternatively, non-oxygen contained defect sites on the basal plane, as well as at the vicinity of wrinkled and folded areas within the NS, can function as NPs nucleation centers[36,39]. This is due to the NS local morphology change, which could efficiently trap the precursor molecules and thus function as nucleation centers for NPs growth. Further work is currently under progress in order to elucidate the exact mechanism behind the formation of NPs onto NSs.

The interest and the application of 2D materials in various building blocks of thin film solar cell technology, has been reported quite extensively[40,41,42,43,44,45,46,47]. Among the strategies adopted to facilitate the energy cascade procedure and promote the transport of light generated charge carriers to the respective electrodes is the introduction of a third component into the photoactive binary layer, resulting in the formation of a ternary blend structure device.[48,49] The motivation behind this approach is the insertion of a material having its highest occupied molecular orbital (HOMO) and lowest unoccupied molecular orbital (LUMO) between the HOMO and LUMO of the polymer and the fullerene. This material can act either as a secondary donor or acceptor material, offering an extra interface for exciton dissociation and charge transfer.[50]

3.2 Fabrication of ternary OPV devices

Semiconductor NS might be promising materials for light harvesting applications due to their unique electrical and optical properties, as well as suitable bandgap values for energetically favorable electron transfer from the polymer donor.[51] Moreover, further improvement in OPVs performance can be achieved via the use of hybrid assemblies based on NS combined with plasmonic metallic NPs.[18,52,53,54,55] In this context, the laser-generated NS-NPs assemblies developed in this work may be suitable to be used as the energy cascade material in ternary OPVs, leading to increased performance, through improved optical absorption due to the NPs, and to improved excitons dissociation and charge collection due to the 2D NS. As a proof of concept, the performance of a ternary OPV[48] based on the addition of NS-Au assemblies into a PCDTBT: $PC_{71}BM$ BHJ layer was investigated. It should be noted that WS_2 and MoS_2 were chosen among the various 2D materials used here, due to its perfect energy levels[56] matching with the state of the art polymer donors used in OPVs. On the contrary, GO[57] and BN[58] are insulating materials and therefore fail to facilitate charge transfer in ternary OPV cells.

The relative position of the additive component energy levels with respect to the electronic levels of the donor and the acceptor materials determines the performance of the ternary solar cell configuration. For this purpose, the HOMO and LUMO levels of WS_2, WS_2-Au, MoS_2 and MoS_2-Au were measured by cyclic voltammetry. The measurements were conducted in a three electrode apparatus, using a Pt foil as the counter electrode and a Ag/AgCl electrode as the reference one. The voltammetric behaviors of the different materials tested in acetonitrile (CH_3CN) using 0.1 M tetrabutylammonium hexafluorophosphate (TBAPF6) as the electrolyte at a scan rate of 100 mV s^{-1} are demonstrated in **Figure S12**. The respective bands were calculated using previously reported formulas[59]. The WS_2 valence band position is approximately at -5.75 eV, calculated from the oxidation peak onset (0.65 V), while its conduction band extracted from the onset of the reduction peak (-0.97 V) is positioned at -4.13 eV. While, the MoS_2 valence band position is approximately at -6.19 eV, calculated from the oxidation peak onset (1.09 V), while its conduction band extracted from the onset of the reduction peak (-0.89 V) is positioned at -4.21 eV. The above measurements are in agreement with previously reported values.[56] The decoration of WS_2 NS with Au NPs had no effect on the measured energy levels, as indicated by the slight change in the oxidation and reduction peaks in **Figure S12** (top). While, the decoration of MoS_2 NS with Au NPs slightly affected the MoS_2 energy levels, as indicated by the slight change in the oxidation and reduction peaks in Figure S12 (bottom), leading to valence band value of -6.31 eV and conduction band value of -4.35 eV.

Figures 5A and **B** depict the device architecture and the energy levels of the components of the WS_2 NS-based devices. It can be observed that the excitons created into PCDTBT can diffuse to both PCDTBT:WS_2-Au and PCDTBT:$PC_{71}BM$ interfaces. Moreover, the conduction band of WS_2-Au is located between the LUMO levels of PCDTBT and $PC_{71}BM$, acting as energy intermediate step, so that the electrons can be transferred towards the cathode via this energetic cascade pathway. It can be concluded that the energy levels of WS_2 perfectly match the energy levels of PCDTBT-donor and $PC_{71}BM$-acceptor, acting as an efficient electron-cascade material. On the contrary, as shown in Figure S16, the conduction and valence band of MoS_2 and MoS_2-Au NS do not lie between the HOMO and LUMO levels of PCDTBT and $PC_{71}BM$. Therefore this material is not expected to improve charge transfer in ternary OPVs. Indeed, ternary OPV devices incorporating GO, BN and MoS_2 NS and their derivatives with NPs showed deteriorated OPV performance, compared to conventional ones (results not shown).

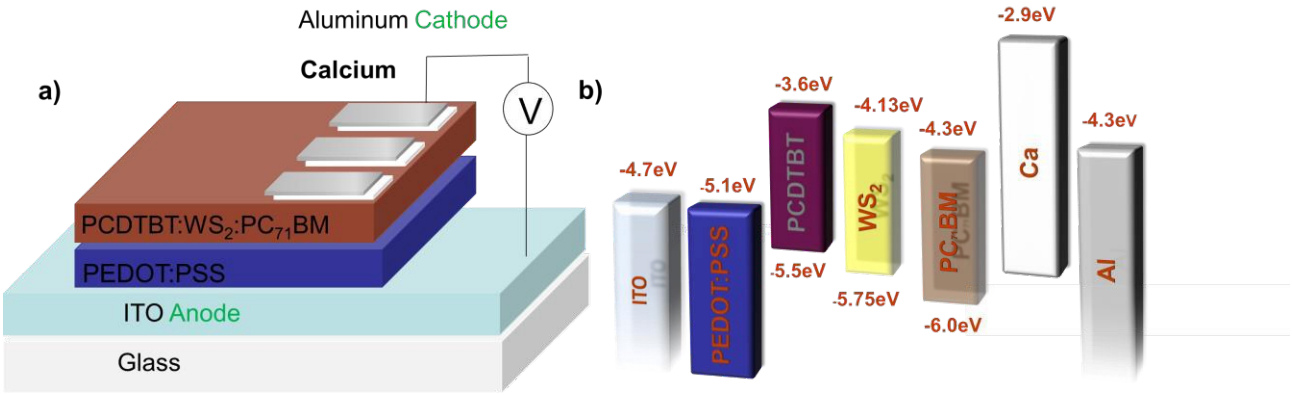

Figure 5. A) Schematic illustration of the sandwich-type BHJ solar cell; B) Energy level diagram of the ternary OPV cell incorporating WS_2-Au NS, showing the energy bands of the different components.

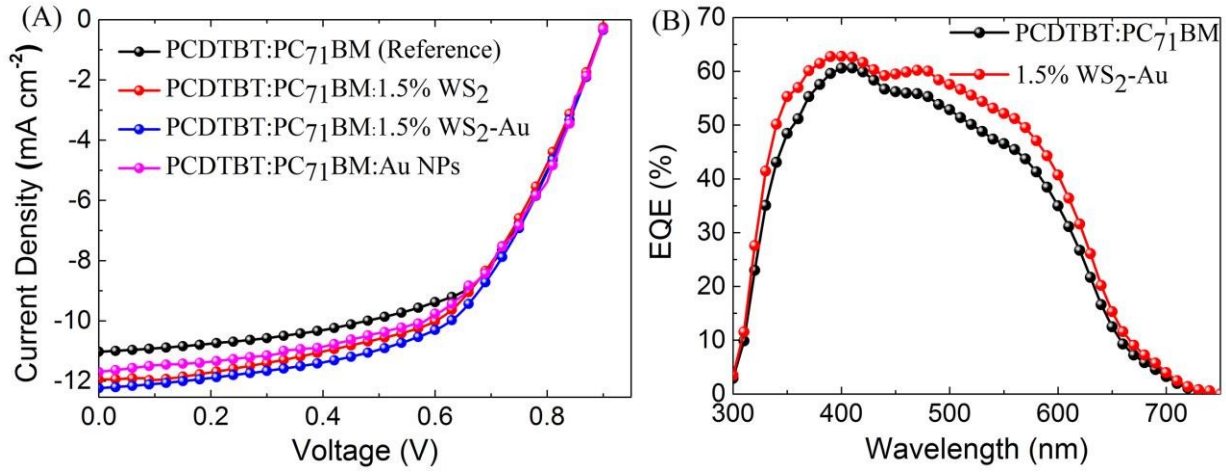

Figure 6. (A) *J-V* characteristics under 1 sun illumination (100 mW cm^{-2}) for the optimized devices incorporating the reference PCDTBT:$PC_{71}BM$, the PCDTBT:Au:$PC_{71}BM$, the PCDTBT:WS_2-Au:$PC_{71}BM$ and the PCDTBT:WS_2-Au:$PC_{71}BM$ blends. (B) IPCE spectra for the control device and the one containing the WS_2-Au assemblies as a ternary component.

The effect of WS_2 and WS_2-NPs assemblies on the performance of BHJ solar cells was investigated by altering the additive content into the photoactive layer. In both cases the optimum additive content was found to be 1.5% v/v. **Figure 6A** demonstrates the current density-voltage (J-V) curves of the best-performed devices in each case for the four different active layers studied, namely PCDTBT:$PC_{71}BM$ (reference), PCDBT:Au:$PC_{71}BM$, PCDBT:WS_2:$PC_{71}BM$ and PCDBT:WS_2-Au:$PC_{71}BM$. While, **Table 1** summarizes the respective photovoltaic

characteristics. An enhancement of the PCE of the optimized PCDTBT:WS_2:$PC_{71}BM$ based device, compared to the reference one, was observed. Specifically, the PCE increased from 5.6% to 6.1%, showing an improvement of 8%, attributed to the increase of the J_{sc}. The latter is caused by improved charge-carrier separation, transportation and collection. However, PCE was further enhanced for the optimized PCDTBT:WS_2-Au:$PC_{71}BM$ based devices, showing an improvement of 12.5% compared to the reference. The performance of such devices was also superior to the optimized PCDBT:Au:$PC_{71}BM$ based ones.

Table 1. Average photovoltaic characteristics for binary and ternary OPV devices with WS_2 NSs, Au NPs and different WS_2-Au NSs contents, as additives. To account for experimental errors, the reported averages for each case are taken for 10 identical devices, consisting of six cells each.

Device structure	J_{SC} (mA cm^{-2})	V_{OC} (V)	FF (%)	PCE (%)
PCDTBT:$PC_{71}BM$	10.6±0.1	0.89±0.1	60.2±0.3	5.6±0.1
1.5% (v/v) WS_2	11.9±0.2	0.87±0.1	59.1±0.2	6.1±0.1
PCDTBT:$PC_{71}BM$-Au	11.7±0.2	0.88±0.1	59.2±0.3	6.1±0.1
1.5% (v/v) WS_2-Au	12.3±0.2	0.89±0.1	58.4±0.2	6.3±0.1
2.5% (v/v) WS_2-Au	10.8±0.14	0.86±0.1	57.0±0.4	5.2±0.2

To investigate the origin of this additional enhancement, the UV-Vis absorption spectra of PCDTBT:$PC_{71}BM$ films with and without the presence of WS_2 (1.5 %) and WS_2-Au (1.5 %) were measured and are presented in **Figure S13**. It is clear that the incorporation of both WS_2 (1.5 %) and WS_2-Au NS enhances the light harvesting of the active layer, compared to the reference film, in a broad wavelength range (380 nm-430 nm), indicating the presence of light scattering effects. This complies with the TEM images of the respective NS shown in **Figure 3B.** Besides this the spectrum of the WS_2-Au based film shows an enhancement in the wavelength region from 480 to 600 nm, which is consistent with the SPR peak of the WS_2-Au assemblies shown in **Fig. 4D**. Therefore, the absorption spectra indicate that the SPR of the WS_2-Au

nanocomposites may be responsible for the additional improvement in the OPV device performance.

Further insight into the light harvesting effects observed is provided by the external quantum efficiency (EQE) spectra of the reference and WS_2-Au based devices respectively, presented in **Figure 6B**. It can be observed that, although PCE for the WS_2-Au based OPV is increased, compared to the reference, in the entire wavelength range, the enhancement is more pronounced in the range 470nm-600nm. This observation complies with that obtained from the absorption spectra analysis and further supports the indication of SPR enhancement effect due to the presense of Au NPs onto the WS_2 nanosheets.

In summary, our results presented above indicate that the efficiency enhancement in the case of the WS_2-based ternary blend, can be attributed to superior charge transport properties inside the photoactive layer, compared to the binary active layer, due to the energy levels offset between the polymer and the WS_2 intermediate component. The additional improvement in the performance of the ternary devices incorporating WS_2-Au assemblies as the third component may be due to SPR-assisted enhanced generation of excitons. It can be concluded that the application of hybrid WS_2-NPs materials is dually beneficial in ternary OPV architecture.

The deterioration of the OPV performance for higher WS_2-Au content into the active medium can be attributed to additive-induced changes in the blend morphology. It is well reported that carrier scattering increases with active layer roughness, giving rise to inefficient collection of the photon-generated carriers from the respective electrodes.[5] In order to investigate this we have performed atomic force microscopy (AFM) measurements of the reference binary and the ternary layers, shown in **Figure S14**. Such measurements demonstrate that the lowest roughness is obtained for the layers incorporating 1.5% (v/v) WS_2 NS and 1.5% (v/v) WS_2-Au NS respectively (rms roughnesses of 0.573 nm and 0.576 nm respectively). On the contrary, the addition of higher NS concentrations leads to a corresponding increase in the layer roughness, giving rise to the degradation of the donor/acceptor interfaces, and in turn of the OPV performance.

4. Conclusions

In summary, we have demonstrated a facile, fast, in situ synthesis of 2D NS-NPs assemblies, via laser induced grafting of metallic NPs onto NS in solution. This is a simple, one-step process,

performed at room temperature and does not require any catalysts or surfactant agents. Furthermore, it can be universally applied for practically any 2D material, giving rise to various combinations of NS-NPs assemblies. As a proof of the potential application of such assemblies, the incorporation of WS_2-Au NPs into the photoactive layer of ternary BHJ OPVs was demonstrated. The results revealed a noticeable enhancement in the photocurrent and the PCE of the respective OPV devices, attributed to the efficient synergy of plasmon enhanced absorption of Au NPs with the superior charge transport properties due to the energy levels matching between the polymer and the intermediate WS_2 NS component. Undoubtedly, this is a useful approach towards extending the spectral range of enhanced light harvesting in OPVs. The rather simple and scalable method provides unique opportunities for the cost-effective synthesis of bulk amounts of NS-NPs assemblies in solution for various applications, including printable optoelectronic devices.

Acknowledgements

The research leading to these results has received funding from the European Union Seventh Framework Programme under grant agreement n°604391 Graphene Flagship. It is also partially supported by the Integrated Initiative of European Laser Research Infrastructures LASERLAB-II (Grant Agreement No. 228334).

References

[1] K.S. Novoselov, A.K. Geim, S.V. Morozov, D. Jiang, Y. Zhang, S.V. Dubonos, I.V. Grigorieva and A.A. Firsov, *Science*, 2004, **306**, 666 -669.

[2] Y. Li and J.W. Connell, *Nanoscale*, 2012, **4**, 6908-6939.

[3] Y. Kubota, K. Watanabe, O. Tsuda and T. Taniguchi, *Science*, 2007, **317**, 932-934.

[4] C.R. Dean, A.F. Young, I. Meric, C.Lee, L. Wang, S. Sorgenfrei, K. Watanabe, T. Taniguchi, P. Kim, K. L. Shepard and J. Hone, *Nat. Nanotechnology*, 2010, **5**, 722-726.

[5] Q. H. Wang, K. K. Zadeh, A. Kis, J. N. Coleman and M. S. Strano, *Nat. Nanotechnology*, 2012, **7**, 699-712.

[6] M. Chhowalla, H. S. Shin; G. Eda, L.-J. Li; K. P. Loh and H. Zhang, *Nat. Chem.* 2013, **5**, 263−275.

[7] A. Splendiani, L. Sun, Y. Zhang, T. Li, J. Kim, C. Y. Chim, G. Galli and F. Wang, *Nano Lett.* 2010, **10**, 1271–1275.

[8] Y.-H. Su, Y.-F. Ke, S.-L. Cai and Q.-Y. Yao, *Light: Sci. & Appl.*, 2012, **1**, e14, doi:10.1038/lsa.2012.14

[9] H. Zhang, Y. Sun, S. Gao, J. Zhang, H. Zhang and D. Song, *Small*, 2013, **9**, 2537–2540.

[10] J. N. Anker, W. P. Hall, O. Lyandres, N. C. Shah, J. Zhao and R. P. Van Duyne, *Nat. Mater.*, 2008, **7**, 442 – 453.

[11] H. Jing, Q. Zhang, N. Large, C. Yu, D.A. Blom, P. Nordlander and H. Wang, N*ano Lett.*, 2014, **14 (6),** 3674–3682.

[12] X. Zhang, X. Ke, A. Du and H. Zhu, *Sci. Rep.*, 2014, **4**, 3805.

[13] S. Linic, U. Aslam, C. Boerigter and M. Morabito, *Nat. Mat.*, 2015 **14**, 567–576.

[14] X. Dong, Y. Shi, W. Huang, P. Chen and L. Li, *Adv. Mater.*, 2010, **22**, 1649-1653.

[15] S. He, K.-K. Liu, S. Su, J. Yan, X. Mao, D. Wang, Y. He, L.-J. Li, S. Song and C. Fan, *Anal. Chem.*, 2012, **84**, 4622 – 4627.

[16] F. Huang and J. J. Baumberg, *Nano Lett.*, 2010, **10**, 1787 – 1792.

[17] Y. C. Lu, Z. Xu, H. A. Gasteiger, S. Chen, K. Hamad-Schifferli and Y. Shao-Horn, *J. Am. Chem. Soc.*, 2010, **132**, 12170 – 12171.

[18] E. Stratakis and E. Kymakis, , *Mater. Today*, 2013, **16**, 133-146.

[19] M. Sygletou, G. Kakavelakis, B. Paci, A. Generosi, E. Kymakis and E. Stratakis, *ACS Appl. Mater. Interfaces*, 2015, DOI: 10.1021/acsami.5b03970.

[20] G. D. Spyropoulos, M. M. Stylianakis, E. Stratakis and E. Kymakis, *Appl. Phys. Lett.*, 2012, **100**, 213904.

[21] G. Kakavelakis, E. Stratakis and E. Kymakis, *Chem. Commun.*, 2014, **50,** 5285 – 5287.

[22] M. Krassas, G. Kakavelakis, M. M. Stylianakis, N. Vaenas, E. Stratakis , E. Kymakis , *RSC Adv.*, 2015, **5**, 71704-71708.

[23] G. Kakavelakis, E. Stratakis and E. Kymakis,, *RSC Adv.*, 2013, **3** , 16288-16291.

[24] F. Bonaccorso, N. Balis, M. M. Stylianakis, M. Savarese, C. Adamo, M. Gemmi, V. Pellegrini, E. Stratakis, E. Kymakis, (2015), *Adv. Func. Mater.*, 25, 5, 3870-3880

[25] Y. Shi, J.K. Huang, L. Jin, Y.T. Hsu, S. Yu, L.J. Li and H.Y. Yang, *Sci. Rep.*, 2013, **3**, 1-7.

[26] Z. Y. Yin, B. Chen, M. Bosman, X. H. Cao, J. Z. Chen, B. Zheng and H. Zhang, *Small*, 2014, **10**, 3537-3543.

[27] A. Alahgholipour Omrani and N. Taghavinia, *Appl. Surf. Sci.*, 2012, **258**, 2373 – 2377.

[28] S. Moussa, G. Atkinson, M. S. El-Shall, A. Shehata, K. M. AbouZeid and M. B. Mohamed, *J. Mater. Chem.,* 2011, **21**, 9608-9619.

[29] S. Moussa, A. R. Siamaki, B. F. Gupton and M. S. El-Shall, *ACS Catalysis*, 2012, **2**, 145-154.

[30] A. F. Zedan, S. Moussa, J. Terner, G. Atkinson and M. S. El-Shall, *ACS Nano*, 2013, **7**, 627-636.

[31] M. J. Meagher, B. Leone, T. L. Turnbull, R. D. Ross, Z. Zhang and R. K. Roeder, *Journals of Nanoparticle Research*, 2013, **15**, 1-10.

[32] J. J. Mock, M. Barbic, D.R. Smith, D.A. Schultz and S. Schultz, *J. Chem. Phys.*, 2002, **116**, 6755 – 6759.

[33] S. K. Mandal, R. K. Roy and A. K. Pal, *J. Phys. D*, 2003, **36**, 261-265.

[34] S. Reich, A.C. Ferrari, R. Arenal, A. Loiseau, I. Bello, J. Robertson, *Phys. Rev. B*, 2005, **71**, 205201.

[35] L. Guardia, S. Villar-Rodil, J. I. Paredes, R. R. Rodríguez, A. Martínez-Alonso and J. M. D. Tascón, *Carbon,* 2012, **50**, 1014-1024.

[36] Y. Shi, J.-K. Huang, L. Jin, Y.-T. Hsu, S. F.Yu, L.-J. Li and H. Y.Yang, *Sci. Rep.* 2013, **3**, 1839.

[37] G. Goncalves, P. A. A. P. Marques, C. M. Granadeiro, H. I. S. Nogueira, M. K. Singh and J. Grácio, *Chemistry of Materials*, 2009, **21**, 4796-4802.

[38] J. Zhu , Y. Shen, A. Xie, L. Qiu, Q. Zhang and S. Zhang*, J. Phys. Chem. C*, 2007, **111**, 7629-7633.

[39] K. K. Kim, A. Reina, Y. Shi, H. Park, L. J. Li, Y. H. Lee and J. Kong, *Nanotechnology*, 2010, **21**, 285205.

[40] E. Kymakis, K. Savva, M. M. Stylianakis, C. Fotakis, E. Stratakis, *Adv. Funct.. Mater.* 2013, **23**, 2742.

[41] E. Stratakis, M. M. Stylianakis, E. Koudoumas, E. Kymakis, *Nanoscale* (2013) **5**, 4144-4150.

[42] E. Stratakis, K. Savva, D. Konios, C. Petridis, E. Kymakis, *Nanoscale* (2014), b, 6925.

[43] M. M. Stylianakis, M. Sygletou, K. Savva, G. Kakavelakis, E. Kymakis and E. Stratakis, *Adv. Opt. Mater.*, 2015, **3**, 596.

[44] G. Kakavelakis, D. Konios, E. Stratakis and E. Kymakis, *Chem. Mater.*, 2014, **26**, 5988.

[45] D. Konios, C. Petridis, G. Kakavelakis, M. Sygletou, K. Savva, E. Stratakis and E. Kymakis, *Adv. Funt. Mater.* 2015, **25**, 2213-2221.

[46] Z. Liu, S. P. Lau and F. Yan, *Chem. Soc. Rev.,* 2015, **44**, 5638-5679.

[47] M. Shanmugam, T. Bansal, C.A. Durcan and B. Yu, *Appl. Phys. Lett.*, 2012, **100**, 153901.

[48] T. Ameri, P. Khoram, J.Min and C.J. Brabec, *Adv. Mater.*, 2013, **25**, 4245 – 4266.

[49] N N. Balis, D. Konios, E. Stratakis and E. Kymakis, *ChemNanoMat*, 2015, DOI: 10.1002/cnma.201500044.

[50] Y.-C. Chen, C.-Y. Hsu, R.Y.-Y. Lin, K.-C. Ho and J.T. Lin, *ChemSusChem*, 2013,. **6**, 20 – 35.

[51] X. Li, W.C.H. Choy, H. Lu, W.E.I. Sha and A.H.P. Ho, *Adv. Func. Mater.*, 2013, **23**, 2728–2735.

[52] M. K. Chuang, S. S. Yang and F. C. Chen, *Materials*, 2015, **8**, 5414-5425.

[53] C. L. Chen, M. K. Chuang, C. H. Chen, C. W. Chu, M. L. Keshtov and F. C. Chen, *Semiconductor Science and Technology*, 2015, **30**, 085013.

[54] M. K. Chuang and F. C. Chen, *ACS Applied Materials & Interfaces*, 2015, **7,** 7397-7405.

[55] M. K. Chuang, S. W. Lin, F. C. Chen, C. W. Chu and C. S. Hsu, *Nanoscale*, 2014, **6**, 1573-1579.

[56] J. Kang, S. Tongay, J. Zhou, J. Li and J. Wu, *J. Appl. Phys.,* 2013, **113**, 143703.

[57] G. Eda, C. Mattevi, H. Yamaguchi, H. K. Kim, and M. Chhowalla, *J. Phys. Chem. C*, 2009, **113**, 15768-15771

[58] M. P. Levendorf, C.-J. Kim, L. Brown, P. Y. Huang, R. W. Havener, D. A. Muller and J. Park, *Nature* 2012, **488**, 627-632

[59] C. M. Cardona, W. Li, A. E. Kaifer, D. Stockdale and G.C. Bazan, *Adv. Mater.*, 2011, **23**, 2367.